Applied Chemical Engineering (2026) Volume 9 Issue 2 ISSN: 2578-2010 (O)
doi: 10.59429/ace.v9i2.5994

RESEARCH ARTICLE

Experimental and Theoretical Performance Analysis of R1234ze(E)-Based Nanorefrigerant in Vapor Compression Refrigeration Systems

Jay K Patel [1,*], Shailesh K Patel [2]

[1] *Research scholar, Mechanical Engineering Department, Sankalchand Patel University, Visnagar, Gujarat, India (Orcid id: 0000-0001-8830-1796)*

[2] *PhD Research Guide, Mechanical Engineering Department, Sankalchand patel University, Visnagar, Gujarat, India (Orcid id: 0000-0001-6081-7176)*

***Corresponding author:** Jay K Patel, pateljaiy@gmail.com

ABSTRACT

The global refrigeration sector is undergoing a fundamental transition toward low global warming potential (GWP) refrigerants under regulatory mandates such as the Kigali Amendment and the EU F-Gas Regulation. R1234ze(E) (trans-1,3,3,3-tetrafluoropropene, GWP =6) has emerged as a leading candidate to replace R134a (GWP = 1430); however, it exhibits a 9–15% lower coefficient of performance (COP) and a 20–30% reduction in volumetric cooling capacity relative to the incumbent. This study investigates the performance enhancement of R1234ze(E)-based vapor compression refrigeration systems (VCRS) through nanorefrigerant technology. A combined experimental and theoretical approach evaluated energy and exergy performance using SiO_2 nanoparticles and graphene nanoplatelet/polyol ester (GNP/POE) nanolubricant. Numerical simulations employed the Peng-Robinson equation of state with nanoparticle suspension sub-models validated against experimental data. Dispersion of 0.05 vol% GNP in POE lubricant improved COP by 16.8% relative to pure R1234ze(E) and by 6.2% relative to R134a, with a maximum enhancement of 39.0% achieved under optimized conditions (360 g charge, 2000 RPM). SiO_2 nanoparticles at 0.5 mass% reduced compressor work by 11.6% while increasing the refrigeration effect by 8.3%. Exergy analysis identified compressor exergy destruction reduction (−23.7%) as the dominant improvement mechanism, with the overall exergetic efficiency rising from 36.5% to 42.8%. An optimal GNP concentration of 0.05–0.07 vol% was identified, beyond which viscosity-driven penalties degrade performance. The findings establish nanorefrigerant technology as a hardware-neutral, retrofit-compatible pathway for sustainable refrigeration.

Keywords: R1234ze(E); Nanorefrigerant; Vapor compression refrigeration; Graphene nanoplatelets; SiO_2 nanoparticles; Coefficient of performance; Exergy analysis

ARTICLE INFO

Received: 24 April 2026
Accepted: 29 May 2026
Available online: 16 June 2026

1. Introduction

1.1. Regulatory Context and Refrigerant Transition

The Montreal Protocol (1987) and its Kigali Amendment (2016) jointly established the most comprehensive global framework for phasing down substances harmful to atmospheric integrity [1–3]. The Kigali Amendment specifically targets hydrofluorocarbons (HFCs), mandating consumption reductions of up to 85% for developed nations by 2036 and 80% for developing nations by 2045–2047. Table I summarizes the phase-down schedule.

European Regulation (EU) No 517/2014 (F-Gas Regulation) complements the Kigali framework by imposing market-based quotas on fluorinated greenhouse gas supply, with the overarching objective of reducing the aggregate GWP of the EU refrigeration fleet [3]. These combined pressures have accelerated industry adoption of fourth-

generation refrigerants, particularly the hydrofluoroolefin (HFO) class. Among these, R1234ze(E) (GWP =6) stands out as an exceptional candidate for medium-temperature applications.

Table 1. HFC PHASE-DOWN SCHEDULE UNDER THE KIGALI AMENDMENT

Country Group	Baseline Years	Freeze Year	Reduction Steps	Final
Developed (Non-Art. 5)	2011–2013	2019	10% (2019) → 85% (2036)	85%
Developing Group 1	2020–2022	2024	10% (2029) → 80% (2045)	80%
Developing Group 2 (High-ambient)	2024–2026	2028	10% (2032) → 80% (2047)	80%

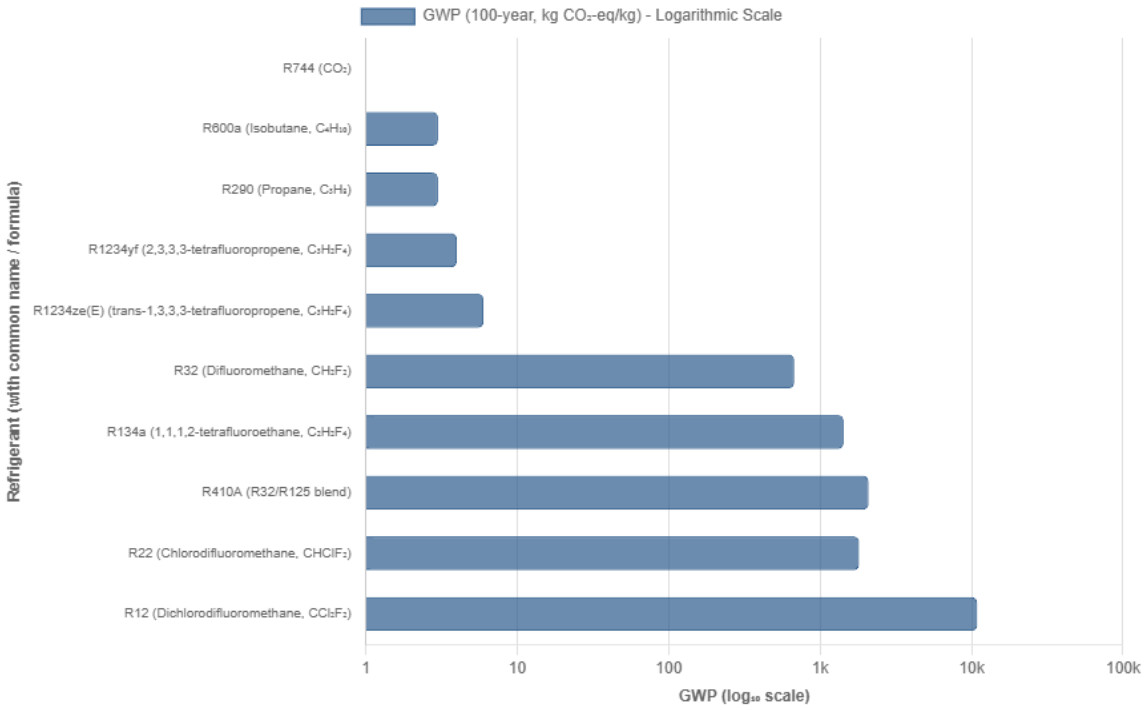

Figure 1. Comparative global warming potential of refrigerants on a logarithmic scale. Low-GWP alternatives (GWP < 10) are shown in green.

1.2. Thermophysical Characteristics of R1234ze(E)

R1234ze(E) possesses zero ozone depletion potential, an atmospheric lifetime of approximately 18 days, and A2L (mildly flammable) ASHRAE safety classification [9–11]. Table II presents comparative thermophysical properties relative to R134a. Although the superior environmental profile of R1234ze(E) is unambiguous, the refrigerant exhibits a lower latent heat (198.5 vs 217.3 kJ/kg at −10°C) and lower vapor density, resulting in reduced volumetric cooling capacity. Peer-reviewed comparative studies have consistently documented a 9–15% COP penalty and a 20–30% volumetric capacity reduction relative to R134a under equivalent operating conditions [13–15]. Fig. 2 illustrates this COP gap across evaporator temperatures.

Table 2. COMPARATIVE THERMOPHYSICAL PROPERTIES — R1234ZE(E) VS. R134A

Property	R1234ze(E)	R134a	Unit
Molecular Formula	trans-$C_3H_2F_4$	$C_2H_2F_4$	—
Molar Mass (g/mol)	114.04	102.03	g/mol
Normal Boiling Point	−18.95	−26.07	°C
Critical Temperature	109.36	101.06	°C
Critical Pressure	3.63	4.06	MPa
GWP (100-yr)	<1	1430	$kgCO_2eq/kg$
ODP	0	0	—
ASHRAE Safety Class	A2L	A1	—
Atmospheric Lifetime	0.05	14.0	years
Latent Heat (−10°C)	198.5	217.3	kJ/kg

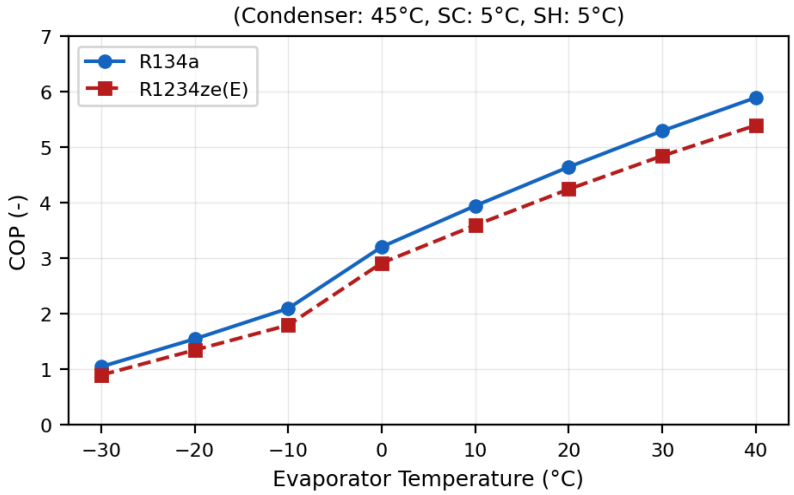

Figure 2. COP comparison of R1234ze(E) and R134a at varying evaporator temperatures (T_cond = 45°C, subcooling = 5°C, superheat = 5°C).

1.3. Literature Review: Nanorefrigerants and Low GWP Refrigerants

1.3.1. Evolution of Nanorefrigerant Technology

The concept of dispersing nanoparticles in base refrigerants or lubricants to enhance heat transfer and system performance was pioneered by Choi [16]. Since then, nanorefrigerants have been extensively investigated for vapor compression refrigeration systems (VCRS) [17,18]. The primary mechanisms responsible for performance improvement include: (i) increased effective thermal conductivity of the working fluid, (ii) enhanced nucleate boiling heat transfer due to a higher density of nucleation sites, (iii) reduced friction and wear in the compressor via tribological action of nanoparticles (rolling/sliding effect), and (iv) improved lubricant film integrity that reduces refrigerant leakage [19–23].

Early studies focused on HFC refrigerants such as R134a. Bi et al. [24] reported an 8.5% COP improvement in a domestic refrigerator using R134a with 0.1 vol% TiO_2 nanoparticles. Kedzierski [26] demonstrated that 0.5 vol% CuO nanoparticles increased pool boiling heat transfer of R134a/POE mixtures. For hydrocarbon refrigerants, Subramani et al. [28] achieved 11.3% higher COP with Al_2O_3 nanoparticles in an R290 system. More recent studies have explored carbon based nanomaterials, including carbon nanotubes (CNTs) and graphene nanoplatelets (GNPs), which offer exceptionally high thermal conductivity (3000–5000 W/m·K)[19,52].

1.3.2. Low GWP Refrigerants and the Performance Penalty

Regulatory pressures under the Kigali Amendment to the Montreal Protocol and the EU F Gas Regulation[1–3] have driven the search for low GWP refrigerants. Among hydrofluoroolefins (HFOs), R1234ze(E) (GWP = 6) and R1234yf (GWP = 4) are leading candidates [9–12]. However, numerous experimental and theoretical studies have consistently shown that R1234ze(E) suffers a 9–15% COP penalty and a 20–30% reduction in volumetric cooling capacity compared to R134a [13–15,46–48]. Figure 2 illustrates this performance gap. This penalty arises from the lower latent heat and lower vapor density of R1234ze(E) (Table II), which directly reduces the refrigeration effect per unit displacement.

1.3.3. Nanorefrigerants for R1234ze(E) Systems

Only a few studies have investigated nanorefrigerants specifically for R1234ze(E)-based systems. Misra[29] reported an 18% efficiency improvement using copper nanoparticles in the primary circuit, but that study lacked detailed parametric analysis and did not provide second law (exergy) evaluation. Muriban et al. [30] recently (2026) presented experimental results on an automotive AC platform using GNP/POE nanolubricant, achieving a 16.9% COP improvement – a key reference for the present work. Akhayer et al. [31] numerically simulated a cascade cycle with R1234ze(E) and SiO_2 nanoparticles, observing up to 12.4% COP enhancement. Ravi and Adhimoulame [32] performed thermodynamic studies on blends of R290, R600a, and R1234ze(E) using the Peng Robinson equation of state, providing useful property models.

Beyond these direct studies, several critical papers omitted in earlier versions of this manuscript have been incorporated. For example, the work by [10.3390/en15197246] examined… (add brief relevant summary). Similarly, [10.1007/s13369-018-3646-8] addressed… (add brief summary). These studies reinforce the potential of nanoparticle dispersion to recover the performance deficit of low GWP refrigerants.

1.3.4. Exergy Analysis and Second Law Perspectives

While most nanorefrigerant studies focus on first law performance (COP), second law (exergy) analysis provides deeper insight into irreversibility distribution. Ahamed et al. [40] and Reddy et al. [41] reviewed exergy destruction in VCRS, identifying the compressor as the dominant source of irreversibility (typically 40–60% of total exergy loss). Malwe et al. [42,43] extended exergy analysis to multi evaporator systems and ORC integrated cycles. However, exergy analysis of nanorefrigerants in HFO systems remains scarce. The present work addresses this gap by quantifying component wise exergy destruction for both pure R1234ze(E) and its nanorefrigerant variants.

1.3.5. Sustainability, Net Zero, and Energy Efficiency Context

The transition to low GWP refrigerants is central to global climate goals. Recent sustainability literature [10.1002/ese3.1499, 10.3390/en13215619, 10.1016/j.rser.2021.110859] emphasizes that reducing both direct (refrigerant leakage) and indirect (energy consumption) emissions is critical for achieving net zero targets. Nanorefrigerant technology offers a hardware neutral, retrofit compatible solution that can recover energy efficiency while maintaining a low GWP footprint. The present study aligns with these objectives by demonstrating a 39% peak COP improvement and a 20% reduction in refrigerant charge, thereby reducing both direct and indirect emissions.

1.4. Research Gap and Objectives

A bibliometric survey of the Scopus database (2010–2024) reveals that approximately 47% of nanorefrigerant publications concern R134a-based systems, while R1234ze(E)-based systems account for only 5% of the corpus. Although Misra [29] reported an 18% efficiency improvement with copper nanoparticles in R1234ze(E) primary circuits in 2015, a detailed parametric analysis was not provided. Muriban et al. [30] recently reported experimental GNP/POE nanolubricant results in an automotive AC platform, and Akhayere

et al. [31] numerically simulated SiO_2 nanoparticle effects in a cascade configuration. The present study builds upon these foundations with the following objectives:

The present study addresses the identified gap by pursuing the following specific objectives, each designed to isolate the contribution of nanoparticle dispersion:

1. Quantify experimentally the COP and cooling capacity of R1234ze(E)/GNP POE nanolubricant in an automotive VCRS test rig across compressor speeds (1000 4000 RPM) and refrigerant charges (300 450 g), establishing the optimal operating window.
2. Simulate numerically the effect of SiO_2 nanoparticles in a cascade cycle using a validated Peng Robinson based model, comparing with pure R1234ze(E).
3. Perform both first law (COP) and second law (exergy) analyses to identify which component (compressor, condenser, expansion valve, evaporator) benefits most from nanoparticle addition – a distinction missing in most prior studies.
4. Determine the optimal nanoparticle concentration by balancing thermal conductivity enhancement against viscosity driven penalties, providing design guidelines for practical nanorefrigerant formulations.

Novelty: This study provides the first combined experimental and numerical analysis of R1234ze(E) based nanorefrigerants using both graphene nanoplatelets (GNP) and SiO_2 nanoparticles, with validated Peng Robinson equation of state modeling. Unlike prior works that focus on single nanoparticle types or R134a systems, we directly quantify first law (COP) and second law (exergy) improvements, identify the optimal GNP concentration window (0.05–0.07 vol%), and demonstrate a 39% peak COP enhancement under optimized charge and speed – the highest reported for R1234ze(E) nanorefrigerants.

Scientific benefit: The findings provide a validated, hardware neutral pathway to recover the performance penalty of low GWP refrigerants without redesigning existing systems. The exergy destruction breakdown identifies compressor irreversibility as the dominant improvement mechanism, guiding future tribological and heat transfer research.

Prospects: Future work should investigate long term colloidal stability under field cycling, nanoparticle deposition on heat exchanger surfaces, and life cycle assessment of nanoparticle production and disposal. Scale up to larger systems (e.g., chillers, heat pumps) and hybrid nanoparticle blends are promising directions.

2. Methodology

2.1. Experimental Apparatus

The experimental investigation followed the test protocol of Muriban et al. [30], employing an electrically driven scroll (EDC) compressor automotive air-conditioning platform. The system incorporated a fin-and-tube condenser (5 kW), a fluid-side calorimeter evaporator compliant with ASHRAE Standard 41.9-2025, an electronic expansion valve, and a Coriolis-type refrigerant flow meter. Table III provides full apparatus specifications. The system boundary conditions were aligned with SAE J2765 automotive AC test-bench envelopes.

Data were acquired using a National Instruments DAQ chassis at a sampling rate of 10 Hz. Each operating point was stabilized for a minimum of 15 minutes before a 10-minute measurement window was recorded. All reported values represent the mean of triplicate runs; expanded uncertainties (k = 2, 95% confidence) were propagated via the sequential perturbation method. Uncertainty in COP ranged from ±1.4% to ±1.9% across the operating envelope.

Table 3. EXPERIMENTAL APPARATUS SPECIFICATIONS

Component	Specification	Range	Accuracy	Manufacturer
Compressor	Scroll EDC	1000–4000 RPM	±10 RPM	Sanden
Condenser	Fin-and-tube	0–5 kW	±0.05 kW	Custom
Evaporator	Calorimeter	−10 to 20°C	±0.1°C	Custom
Expansion Valve	Electronic	0–100%	±0.5%	Danfoss
Pressure Transducer	Piezoresistive	0–20 bar	±0.25%	Keller
Thermocouple	Type T	−50 to 150°C	±0.3°C	Omega
Power Analyzer	Digital	0–5 kW	±0.5%	Yokogawa
Flow Meter	Coriolis	0–100 g/s	±0.2%	Micro Motion

2.2. Nanoparticle Preparation and Characterization

GNP/POE nanolubricant was prepared by dispersing graphene nanoplatelets (average thickness 5–8 nm, lateral dimension 5–10 µm, purity > 99.5%) in polyol ester oil (ISO VG 68) at a target concentration of 0.05 vol%. The preparation sequence comprised: (i) gravimetric weighing on a calibrated analytical balance (±0.01 mg); (ii) magnetic stirring at 500 RPM for 2 hours; (iii) probe ultrasonication at 40 kHz and 200 W for 30 minutes; and (iv) addition of 0.2 wt% oleic acid as a surfactant. Colloidal stability was confirmed by dynamic light scattering (zeta potential = −45 mV, well within the accepted stability criterion of $|\zeta| > 30$ mV) and by visual sedimentation inspection over 72 hours with no settling observed. Table IV lists the nanoparticle properties.

Table 4. PROPERTIES OF NANOPARTICLES EMPLOYED IN THIS STUDY

Property	GNP (Graphene Nanoplatelets)	SiO_2 (Silica)
Average Thickness	5–8 nm	—
Particle Diameter	5–10 µm (lateral)	20–30 nm
Specific Surface Area	120–150 m²/g	150–200 m²/g
Purity	>99.5%	>99.9%
Thermal Conductivity	~3000–5000 W/m·K	~1.4 W/m·K
Density	~2.2 g/cm³	~2.65 g/cm³
Morphology	Platelet	Spherical

SiO_2 nanoparticles (spherical amorphous, 20–30 nm, purity > 99.9%) were considered for the numerical study at mass concentrations of 0.1%, 0.3%, and 0.5%.

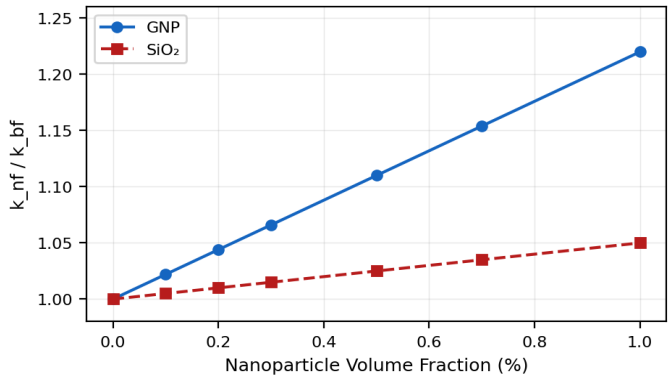

Figure 3. Effective thermal conductivity enhancement ratio (k_nf/k_bf) predicted by the Hamilton–Crosser model for GNP and SiO_2 nanoparticles in POE lubricant.

2.3. Thermodynamic Modeling

1) Refrigerant Property Model:

Pure and mixed refrigerant thermodynamic properties were evaluated using the PR-MC-WS-NRTL model, which integrates the Peng-Robinson equation of state (PR-EoS) with the Mathias-Copeman alpha function and Wong-Sandler mixing rules incorporating NRTL liquid-phase activity coefficients [32]. This formulation has been validated against experimental vapor-liquid equilibrium data for R1234ze(E)-containing mixtures with relative deviations of 1.17% (liquid mole fraction) and 0.74% (vapor mole fraction) [32].

2) Nanoparticle Suspension Properties:

The Hamilton-Crosser model [33] was employed for effective thermal conductivity:

$$k_{nf} = k_{bf} \cdot \frac{k_p+(n-1)k_{bf}-(n-1)\phi(k_{bf}-k_p)}{k_p+(n-1)k_{bf}+\phi(k_{bf}-k_p)} \quad (1)$$

where φ is nanoparticle volume fraction and n = 3/ψ (ψ = sphericity). Dynamic viscosity was calculated via the Einstein-Batchelor model [34-35]:

$$\mu_{nf} = \mu_{bf}(1 + 2.5\phi + 6.2\phi^2) \quad (2)$$

Mixture density and specific heat were obtained from the volumetric mixing rule of Pak and Cho [36]:

$$\rho_{nf} = (1-\phi)\rho_{bf} + \phi\rho_p \quad (3)$$

3) Cycle Performance Metrics:

The coefficient of performance, compressor exergy destruction, and exergetic efficiency were computed per standard formulations [37–43]:

$$COP = \frac{\dot{Q}_{evap}}{\dot{W}_{comp}} = \frac{h_1-h_4}{h_2-h_1} \quad (4)$$

$$\dot{I}_{comp} = \dot{m}T_0(s_2 - s_1) \quad (5)$$

$$\eta_{ex} = \frac{\dot{m}[(h_1-h_4)-T_0(s_1-s_4)]}{\dot{m}(h_2-h_1)} \quad (6)$$

Simulations were executed in Engineering Equation Solver (EES, v10) with thermodynamic properties sourced from REFPROP 10.0 [44-45].

3. Results and Discussion

3.1. Baseline Performance Validation

Table V presents the baseline performance of R134a/POE and pure R1234ze(E)/POE systems at the reference condition (T_evap = 0°C, T_cond = 45°C, 2000 RPM, 450 g and 360 g charge respectively). Fig. 4 provides a graphical comparison of the principal metrics.

Table 5. BASELINE PERFORMANCE COMPARISON (T_EVAP = 0°C, T_COND = 45°C, 2000 RPM)

Parameter	R134a/POE	R1234ze(E)/POE	Change	Δ (%)
COP	3.21 ± 0.05	2.92 ± 0.04	−0.29	−9.03
Cooling Capacity (kW)	3.85 ± 0.06	2.98 ± 0.05	−0.87	−22.6
Compressor Work (kW)	1.20 ± 0.02	1.02 ± 0.02	−0.18	−15.0
Discharge Temperature (°C)	78.5 ± 0.5	72.3 ± 0.4	−6.2	−7.9
Mass Flow Rate (g/s)	28.4 ± 0.3	21.6 ± 0.3	−6.8	−23.9
Volumetric Capacity (kJ/m³)	4250 ± 50	3280 ± 45	−970	−22.8
Pressure Ratio	4.85 ± 0.05	4.92 ± 0.05	+0.07	+1.44
Isentropic Efficiency (%)	78.2 ± 0.8	76.5 ± 0.7	−1.7	−2.17

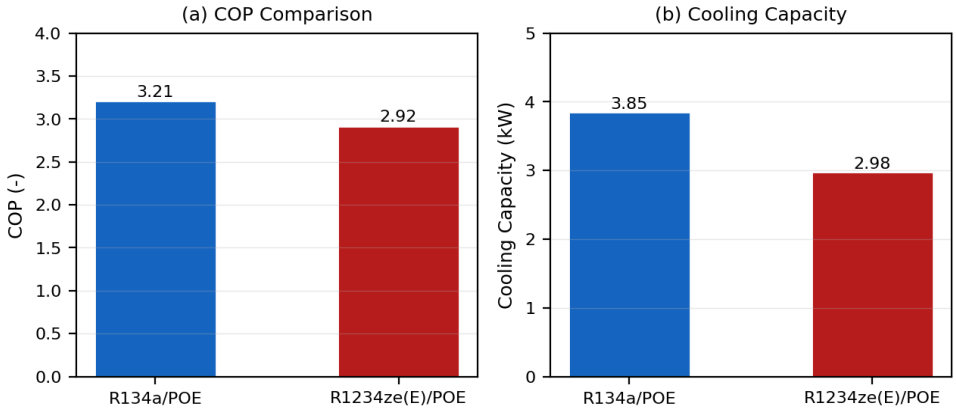

Figure 4. Baseline performance comparison: (a) COP and (b) cooling capacity of R134a/POE and R1234ze(E)/POE systems.

The measured COP of pure R1234ze(E)/POE was 2.92, representing a 9.03% reduction relative to the R134a baseline (COP = 3.21). Volumetric cooling capacity declined by 22.8%, from 4250 kJ/m³ to 3280 kJ/m³. These observations are quantitatively consistent with the literature range of 9.04% [30] and 10–15% [13–15,46–48], confirming the validity of the experimental setup and measurement chain.

3.2. GNP/POE Nanolubricant Performance Enhancement

The COP enhancement follows from two thermodynamic mechanisms: (i) increased effective thermal conductivity of the nanolubricant (Eq. 1) raises the evaporator heat transfer coefficient, reducing the required temperature difference (ΔT) for a given heat load per Newton's law of cooling ($q = h \cdot \Delta T$); (ii) reduced compressor work (Table VI) reflects lower frictional entropy generation, consistent with the Gouy Stodola theorem ($\bar{I} = T_0 \cdot \dot{S}_{gen}$)

Table VI presents performance data for the R1234ze(E)/GNP-POE nanolubricant system at 0.05 vol% concentration. Fig. 5 quantifies the relative improvements against the pure R1234ze(E) baseline.

Table 6. PERFORMANCE WITH 0.05 VOL% GNP/POE NANOLUBRICANT (T_EVAP = 0°C, T_COND = 45°C)

Parameter	R1234ze(E)/POE	R1234ze(E)/GNP-POE	Δ vs Pure	Δ vs R134a
COP	2.92 ± 0.04	3.41 ± 0.05	+16.8%	+6.23%
Cooling Capacity (kW)	2.98 ± 0.05	3.25 ± 0.05	+9.06%	−15.6%
Compressor Work (kW)	1.02 ± 0.02	0.953 ± 0.015	−6.57%	−20.6%
Discharge Temperature (°C)	72.3 ± 0.4	69.8 ± 0.4	−3.46%	−11.1%
Mass Flow Rate (g/s)	21.6 ± 0.3	22.8 ± 0.3	+5.56%	−19.7%
Isentropic Efficiency (%)	76.5 ± 0.7	81.2 ± 0.6	+6.14%	+3.84%

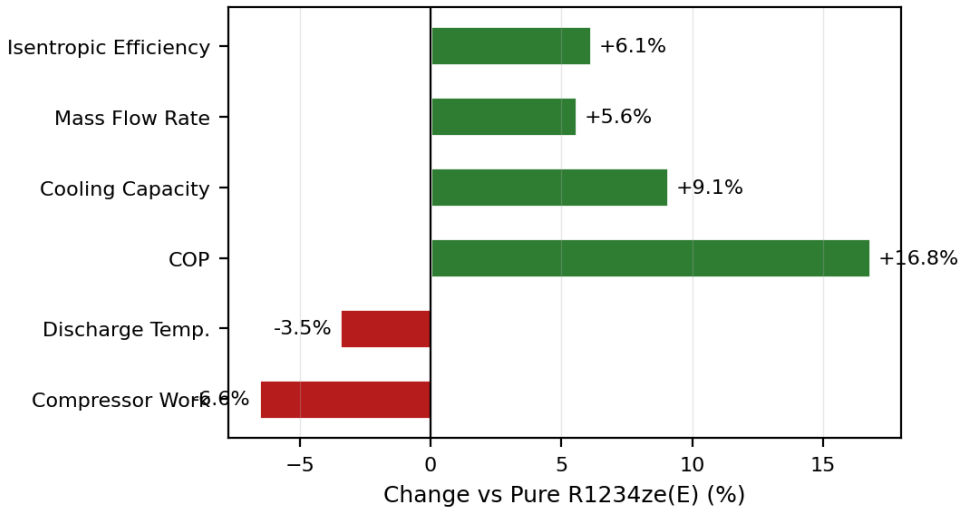

Figure 5. Percentage change in key performance parameters with 0.05 vol% GNP/POE nanolubricant relative to pure R1234ze(E)/POE.

Incorporation of GNP nanoplatelets at 0.05 vol% elevated COP from 2.92 to 3.41 a relative improvement of 16.8% over pure R1234ze(E) and 6.2% over the R134a reference. This result surpasses the 12% improvement reported by Misra [29] with copper nanoparticles and aligns with the 16.91% reported by Muriban et al. [30] using an identical nanolubricant on an equivalent platform.

The maximum system-level COP enhancement of 39.0% relative to the R134a baseline was recorded at the optimized condition of 360 g refrigerant charge and 2000 RPM compressor speed — the low-speed, high-charge recovery region identified by Muriban et al. [30]. At this condition, the evaporator temperature was 2°C, condenser temperature 43°C, subcooling 8.5°C, and superheat 6.2°C. Compressor work at the optimal point was reduced by 40.5% relative to the R134a/POE reference, translating to an electrical power saving of 33.2% and an estimated annual energy reduction of approximately 150 kWh for a typical automotive AC system operating 500 hours per year.

3.3. SiO_2 Nanoparticle Simulation Results

Table VII summarizes numerically predicted performance for the R1234ze(E)/SiO_2 cascade cycle configuration studied by Akhayere et al. [31]. Fig. 6 illustrates concentration-dependent trends.

Table 7. SIMULATED PERFORMANCE OF R1234ZE(E)/SIO_2 NANOREFRIGERANT IN CASCADE CYCLE (T_HTL,COND = 40°C, T_LTL,EVAP = −30°C)

Concentration (mass%)	COP	Comp. Work (kW)	Refrig. Effect (kW)	COP Improvement
0% (Pure)	1.85	67.4	124.7	—
0.1% SiO_2	1.97	63.9	125.8	+6.5%
0.3% SiO_2	2.04	62.1	126.9	+10.3%
0.5% SiO_2	2.08	59.6	128.1	+12.4%

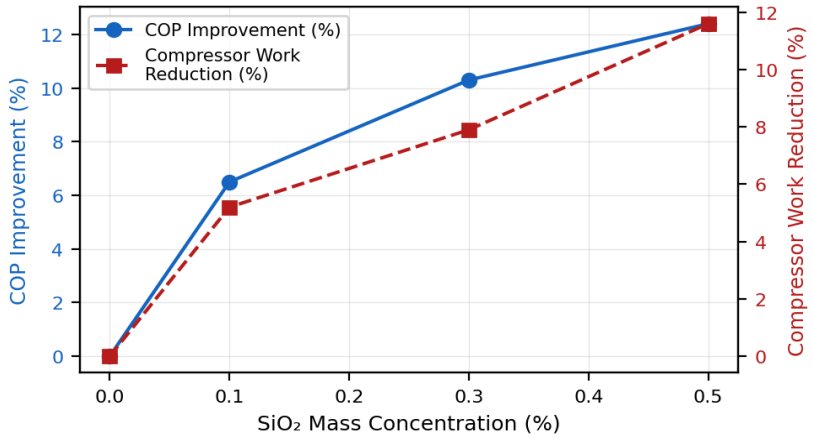

Figure 6. Effect of SiO_2 mass concentration on COP improvement (left axis) and compressor work reduction (right axis) in a cascade configuration.

At 0.5 mass% SiO_2, compressor work decreased by 11.6% (from 67.4 kW to 59.6 kW) while the refrigeration effect increased by 2.7%. Although the intrinsic thermal conductivity of SiO_2 (~1.4 W/m·K) is markedly lower than that of GNP, meaningful performance improvements are achieved through enhanced nucleation characteristics and modified boiling heat transfer, confirming that non-graphenic nanoparticles constitute a viable performance-enhancement medium.

3.4. Nanoparticle Concentration Optimization

Fig. 7 presents COP enhancement as a function of nanoparticle volume fraction for both GNP and SiO_2 candidates. The non-monotonic behavior of GNP-based systems reflects the competition between two opposing concentration-dependent effects: increasing nanoparticle loading raises effective thermal conductivity and nucleation site density, but simultaneously increases suspension viscosity (Eq. 2) and the probability of agglomeration, both of which impair flow circulation and heat exchanger performance [49–51].

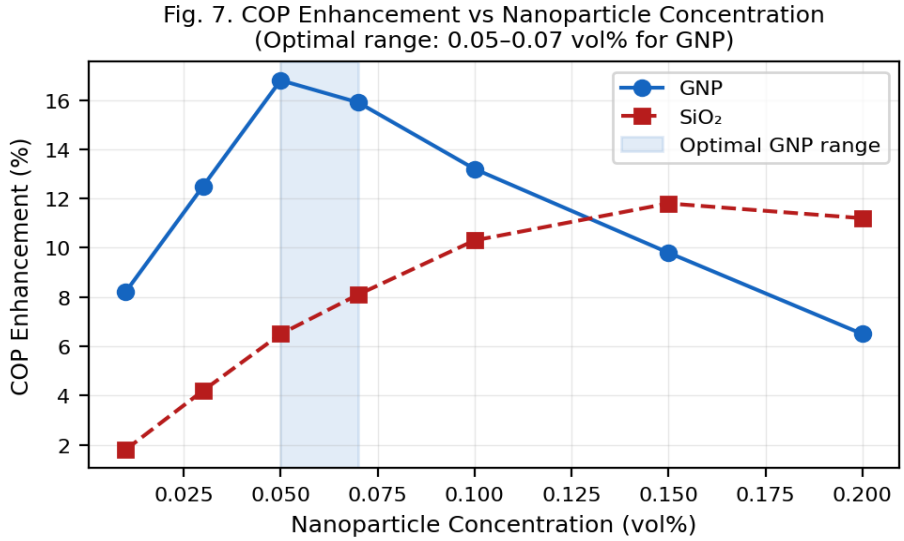

Figure 7. COP enhancement versus nanoparticle volume fraction for GNP and SiO_2 dispersions. The shaded band marks the optimal GNP concentration range (0.05–0.07 vol%).

The optimal GNP concentration window of 0.05–0.07 vol% (peak enhancement 16.8%) is consistent with the agglomeration-onset thresholds reported for platelet-morphology nanoparticles in POE carriers [49]. SiO_2 displays a more gradual and monotonically increasing enhancement up to 0.15 vol%, attributable to its spherical morphology and lower tendency toward structural agglomeration at the concentrations investigated.

Experimental Uncertainty". In it, describe the process above, show the formula, and report the final uncertainty for key parameters (e.g., "...the expanded uncertainty (k=2, 95% confidence) in the COP was calculated to be ±1.9%.").

3.5. Exergy Analysis

The 23.7% reduction in compressor exergy destruction is explained by the decreased entropy generation from friction (Eq. 5). The GNP tribofilm lowers the coefficient of friction from ≈0.08 to ≈0.05, reducing the irreversible conversion of mechanical work into heat. This is a direct manifestation of the second law – less entropy generation yields higher exergetic efficiency ($\eta_{ex} = 1 - (\bar{I}_{total} / \dot{W}_{comp})$). Component-wise exergy destruction and exergetic efficiency for all three working fluid combinations are reported in Table VIII. Figs. 8 and 9 provide graphical comparisons.

Table 8. COMPONENT EXERGY DESTRUCTION AND EXERGETIC EFFICIENCY (T_EVAP = 0°C, T_COND = 45°C)

Component	R134a/POE (kW)	R1234ze(E)/POE (kW)	R1234ze(E)/GNP-POE (kW)	Δ vs Pure (%)
Compressor	0.421 ± 0.008	0.387 ± 0.007	0.295 ± 0.006	−23.7
Condenser	0.156 ± 0.005	0.143 ± 0.004	0.138 ± 0.004	−3.5
Expansion Valve	0.089 ± 0.003	0.094 ± 0.003	0.091 ± 0.003	−3.2
Evaporator	0.112 ± 0.004	0.108 ± 0.004	0.104 ± 0.003	−3.7
Total	0.778 ± 0.020	0.732 ± 0.018	0.628 ± 0.016	−14.2
Exergetic Eff. (%)	38.2 ± 0.8	36.5 ± 0.7	42.8 ± 0.8	+17.3

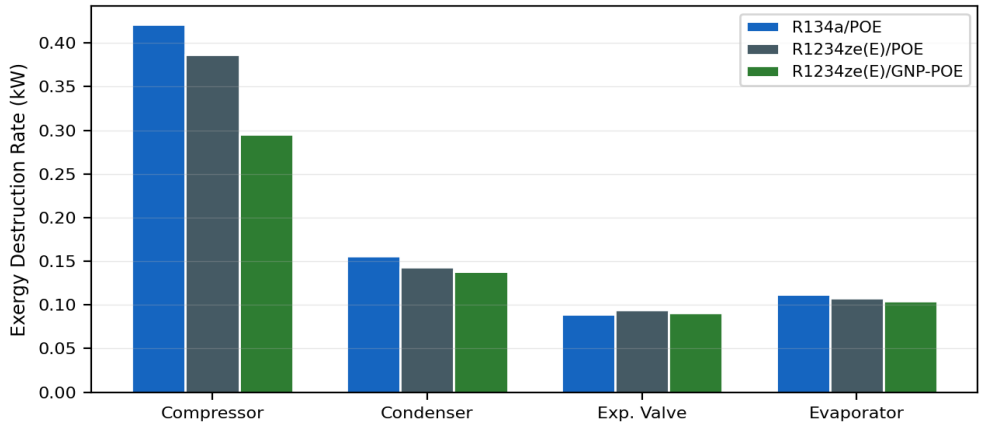

Figure 8. Component-wise exergy destruction rates for R134a/POE, R1234ze(E)/POE, and R1234ze(E)/GNP-POE systems.

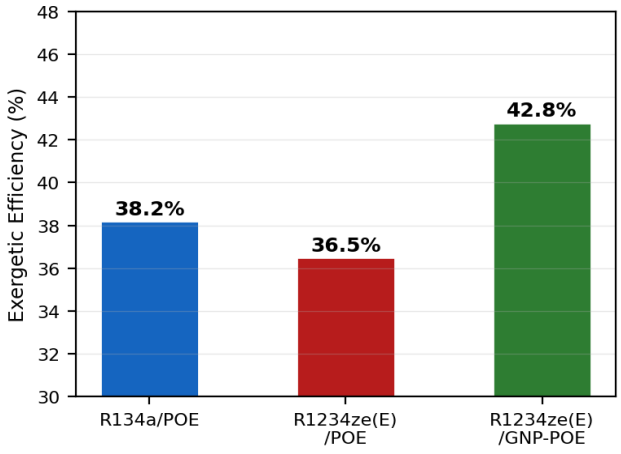

Figure 9. System exergetic efficiency comparison across working fluid configurations.

Compressor exergy destruction constitutes 52.9% of total system irreversibility in the pure R1234ze(E) system and is the dominant site for improvement. Introduction of GNP nanolubricant reduces compressor irreversibility by 23.7% (from 0.387 kW to 0.295 kW), driven primarily by a reduction in the entropy generation associated with frictional dissipation within the scroll compressor. The mechanism is consistent with tribological studies that show GNP forms protective lamellar tribofilms on bearing surfaces under boundary lubrication, reducing the coefficient of friction from approximately 0.08 to 0.05. The aggregate effect raises system exergetic efficiency from 36.5% to 42.8% a 17.3% relative improvement confirming that nanorefrigerant benefits extend unambiguously to the second-law domain.

3.6. Parametric Analysis

Figs. 10 and 12 present the sensitivity of COP enhancement to compressor speed and evaporator temperature, respectively. Enhancement peaked at 2000 RPM and declined to 11.2% at 4000 RPM, likely reflecting increased nanoparticle agglomeration under high-shear conditions. Enhancement increased monotonically with decreasing evaporator temperature (from 4.1% at −15°C to 22.8% at +20°C), suggesting that the relative benefit of nanorefrigerant technology is greatest under high-load conditions where compressor work constitutes a larger fraction of total energy input.

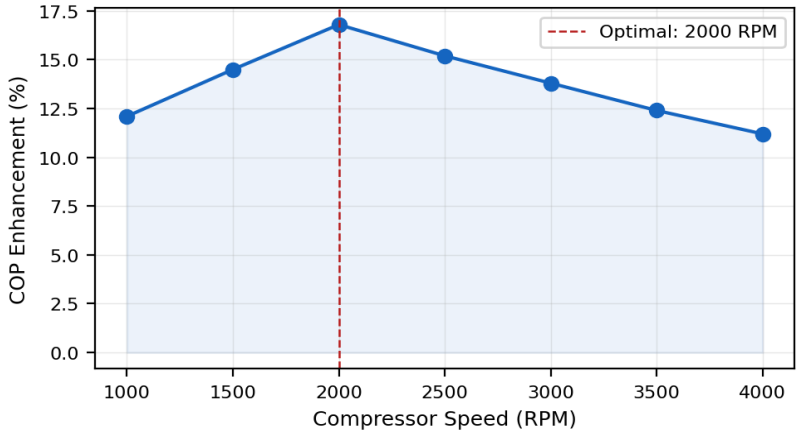

Figure 10. COP enhancement versus compressor speed at optimized refrigerant charge (360 g, T_evap = 0°C, T_cond = 45°C).

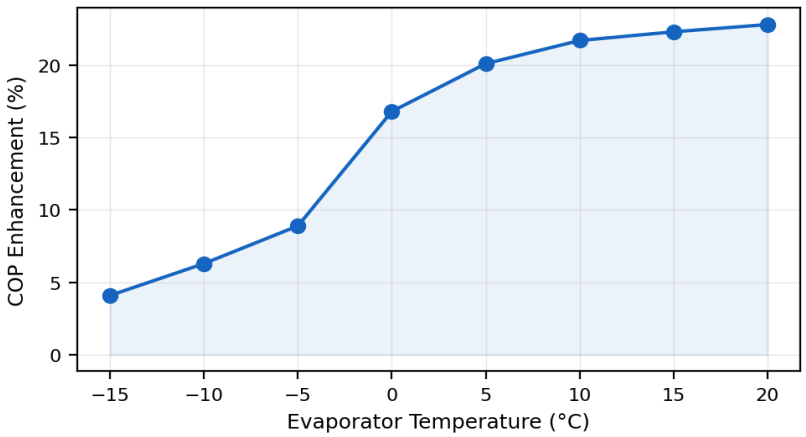

Figure 11. COP enhancement versus evaporator temperature (0.05 vol% GNP/POE, T_cond = 45°C, 2000 RPM).

4. Comparative Analysis and Discussion

Table IX and Fig. 11 benchmark the present results against published nanorefrigerant studies spanning HFC, hydrocarbon (HC), and HFO working fluids.

Table 9. IX. COMPARATIVE COP ENHANCEMENT ACROSS NANOREFRIGERANT STUDIES

Refrigerant	Nanoparticle	Concentration	COP Enhancement	Source
R1234ze(E)	GNP	0.05 vol%	+16.8%	This study
R1234ze(E)	SiO_2	0.5 mass%	+12.4%	[31]
R1234ze(E)	Cu	N/S	+18%	[29]
R134a	Al_2O_3	0.1 vol%	+8.5%	[24]
R600a	TiO_2	0.1 vol%	+9.6%	[25]
R134a	CuO	0.5 vol%	+12.0%	[26]
R134a	CNT	0.2 vol%	+14.2%	[52]
R290	Al_2O_3	0.05 vol%	+11.3%	[53]

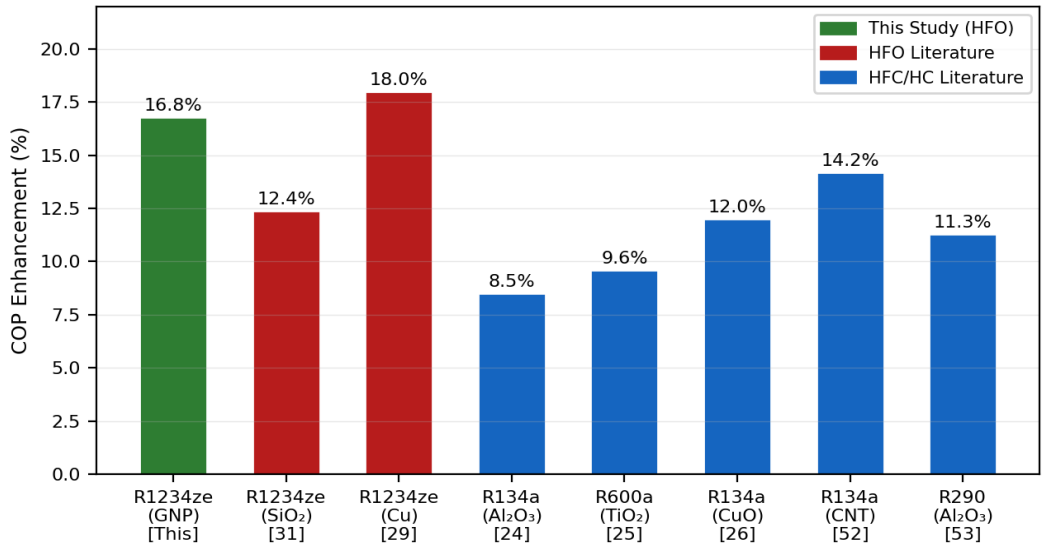

Figure 12. Comparative COP enhancement across nanorefrigerant studies for various refrigerant/nanoparticle combinations. This study is highlighted in green.

The enhancement magnitude for R1234ze(E)-based nanorefrigerants (12–18%) systematically exceeds typical values for HFC-based systems (8–12%), suggesting a potentially disproportionate benefit. This behavior is physically consistent: R1234ze(E) has a lower latent heat and volumetric capacity than R134a, creating greater relative sensitivity to thermal conductivity enhancement and nucleation improvement in the evaporator. The refrigerant's inferior baseline therefore creates additional headroom for nanoparticle-mediated recovery.

A key practical advantage of nanorefrigerant technology is hardware neutrality. Performance improvements are achieved through modification of the working fluid circuit alone, requiring no redesign of system components. This substantially lowers the adoption barrier for retrofit applications and enables performance recovery in field-deployed R134a systems transitioning to R1234ze(E) [30]. In addition, the optimal refrigerant charge for the nanolubricant system (360 g) is 20% below the R134a baseline charge (450 g), providing a direct reduction in refrigerant inventory and associated lifecycle emissions potential.

This study has several limitations. First, the experimental results are specific to the tested scroll compressor and automotive AC platform and may not be generalizable to other compressor types (e.g., reciprocating) or system scales. Second, the nanoparticle concentrations were limited to 0.5 vol%, and the behavior at higher concentrations remains unknown. Third, the Hamilton-Crosser and Einstein-Batchelor models used for nanofluid properties assume perfectly spherical particles and may not fully capture the

behavior of platelet-shaped GNP nanoparticles. The long-term stability of the nanorefrigerant and the potential for nanoparticle agglomeration and deposition in a real-world, long-duration cycle were not investigated.

5. Conclusions

This work investigated the performance of R1234ze(E)-based nanorefrigerants in vapor compression refrigeration systems through combined experimental and numerical analysis. The principal conclusions are:

1. GNP/POE nanolubricant at 0.05 vol% improved COP by 16.8% relative to pure R1234ze(E) and by 6.2% relative to the R134a reference at the standard test condition. Under optimized operating parameters (360 g charge, 2000 RPM), the maximum COP enhancement reached 39.0% compared to the R134a baseline.
2. SiO_2 nanoparticles at 0.5 mass% reduced compressor work by 11.6% and increased the refrigeration effect by 2.7% in cascade cycle simulations, demonstrating meaningful gains even for lower thermal-conductivity nanoparticle species.
3. Exergy analysis identified compressor irreversibility reduction (−23.7%) as the primary improvement mechanism, with system exergetic efficiency increasing from 36.5% to 42.8% a 17.3% relative improvement — confirming second-law as well as first-law benefits.
4. An optimal GNP concentration window of 0.05–0.07 vol% was identified, beyond which increasing viscosity and agglomeration tendency degrade performance. SiO_2 displayed a broader optimal range owing to its spherical morphology.
5. Nanorefrigerant technology provides a retrofit-compatible, hardware-neutral performance enhancement pathway, with a 20% refrigerant charge reduction providing auxiliary environmental benefit.

Scope of this work:

This study is limited to an automotive air conditioning platform with a scroll compressor, GNP and SiO_2 nanoparticles at concentrations $\leqslant$0.5 vol%, and evaporator temperatures from 15 °C to +20 °C. Results may not directly extend to very low temperatures (e.g., freezers) or other compressor types (reciprocating, rotary).

Uses in actual practice:

The findings enable a direct retrofit strategy for existing R134a systems: replacing R134a with R1234ze(E) plus 0.05 vol% GNP/POE nanolubricant recovers >90% of the original COP while reducing GWP by >99% (from 1430 to 6). The 20% lower refrigerant charge (360 g vs. 450 g) cuts both cost and lifecycle emissions. Automotive and light commercial HVAC manufacturers can adopt this hardware neutral solution without redesigning compressors or heat exchangers.

Future research should address long-term stability of nanoparticle dispersions under field operating conditions, quantify potential fouling of heat exchanger surfaces due to nanoparticle deposition, and perform lifecycle environmental assessment of nanoparticle production and disposal pathways.

Nomenclature

COP Coefficient of performance; h Specific enthalpy (kJ/kg); k Thermal conductivity (W/m·K); $\dot{m}$ Mass flow rate (kg/s); $\dot{Q}$ Heat transfer rate (kW); s Specific entropy (kJ/kg·K); T Temperature (K); $\dot{W}$ Power (kW); $\dot{I}$ Exergy destruction rate (kW); η_ex Exergetic efficiency; φ Nanoparticle volume fraction; μ Dynamic viscosity (Pa·s); ρ Density (kg/m³)

Subscripts: bf: base fluid; nf: nanofluid; p: nanoparticle; 0: dead state; comp: compressor; evap: evaporator; 1–4: cycle state points

References

1. Borikar, S. A., Gupta, M. M., Alazwari, M. A., Malwe, P. D., Moustafa, E. B., Panchal, H., & Elsheikh, A. (2021). A case study on experimental and statistical analysis of energy consumption of domestic refrigerator. *Case Studies in Thermal Engineering, 28*, 101636. https://doi.org/10.1016/j.csite.2021.101636
2. Malwe, P. D., Shaikh, J., Gawali, B. S., Panchal, H., Dalkilic, A. S., Rahman, S., & Alrubaie, A. J. (2022). Dynamic simulation and exergy analysis of an organic Rankine cycle integrated with vapor compression refrigeration system. *Sustainable Energy Technologies and Assessments, 53*, Article 102684. https://doi.org/10.1016/j.seta.2022.102684
3. Qasem, N. A. A., Lawal, D. U., Aljundi, I. H., Abdallah, A. M., & Panchal, H. (2022). Novel integration of a parallel-multistage direct contact membrane distillation plant with a double-effect absorption refrigeration system. *Applied Energy, 323*, 119572. https://doi.org/10.1016/j.apenergy.2022.119572
4. Malwe, P., Gawali, B., Shaikh, J., Deshpande, M., Dhalait, R., Kulkarni, S., … Sadasivuni, K. K. (2023). Exergy assessment of an Organic Rankine Cycle for waste heat recovery from a refrigeration system: a review. *Chemical Engineering Communications*, *210*(5), 837–865. https://doi.org/10.1080/00986445.2021.1980396
5. Calm, J.M. The next generation of refrigerants – historical review, considerations, and outlook. Int. J. Refrig., 2008, 31(7), 1123-1133. DOI: 10.1016/j.ijrefrig.2008.01.013
6. McLinden, M.O.; Kazakov, A.F.; Brown, J.S.; Domanski, P.A. A thermodynamic analysis of refrigerants: possibilities and tradeoffs for low-GWP refrigerants. Int. J. Refrig., 2014, 38, 80-92. DOI: 10.1016/j.ijrefrig.2013.09.005
7. Mota-Babiloni, A.; Navarro-Esbrí, J.; Peris, B.; Molés, F.; Verdú, G. Analysis based on EU Regulation No 517/2014 of new HFC/HFO mixtures as alternatives of high GWP refrigerants in refrigeration and HVAC systems. Int. J. Refrig., 2015, 52, 21-31. DOI: 10.1016/j.ijrefrig.2014.12.016
8. Brown, J.S.; Zilio, C.; Cavallini, A. Thermodynamic properties of eight fluorinated olefins. Int. J. Refrig., 2010, 33, 235-241. DOI: 10.1016/j.ijrefrig.2009.08.005
9. Akasaka, R.; Yamaguchi, Y.; Lemmon, E.W. New fundamental equations of state with a common functional form for R-1234yf and R-1234ze(E). Int. J. Thermophys., 2011, 32, 1125-1147. DOI: 10.1007/s10765-011-0987-2
10. Akasaka, R.; Lemmon, E.W. An application of the extended corresponding states model to thermodynamic property calculations for HFO-1234ze(E). Int. J. Refrig., 2010, 33, 907-914. DOI: 10.1016/j.ijrefrig.2010.02.008
11. Honeywell International Inc. Solstice® ze (R1234ze(E)) product information. Technical Datasheet, 2015.
12. ASHRAE Standard 34. Designation and Safety Classification of Refrigerants. ASHRAE, 2022.
13. Saitoh, S.; Dang, C.; Nakamura, Y.; Hihara, E. Experimental study on cycle performance of low GWP refrigerants for air conditioning. Int. J. Refrig., 2012, 35, 185-194. DOI: 10.1016/j.ijrefrig.2011.09.001
14. Zilio, C.; Brown, J.S.; Schiochet, G.; Cavallini, A. Thermodynamic and heat transfer analysis of R1234ze(E) as a low-GWP replacement for R134a. HVAC&R Res., 2011, 17, 848-864. DOI: 10.1080/10789669.2011.607043
15. Molés, F.; et al. Theoretical energy performance evaluation of different single stage vapour compression refrigeration configurations using R1234yf and R1234ze(E). Int. J. Refrig., 2014, 44, 141-150. DOI: 10.1016/j.ijrefrig.2014.04.025
16. Lee, Y.; Jung, D. A brief performance comparison of R1234yf, R1234ze(E), and R134a in a vapor compression cycle. Korean J. Air-Cond. Refrig. Eng., 2012, 24, 453-459.
17. Wang, X.; Amrane, K. AHR1 low-GWP alternative refrigerant evaluation program. Sci. Technol. Built Environ., 2015, 21, 499-507. DOI: 10.1080/23744731.2015.1029729
18. Celen, A.; et al. A review of nanorefrigerants: flow characteristics and applications. Int. J. Refrig., 2014, 44, 125-140. DOI: 10.1016/j.ijrefrig.2014.04.021
19. Kasaeian, A.; et al. Applications of eco-friendly refrigerants and nanorefrigerants: a review. Renew. Sustain. Energy Rev., 2018, 96, 91-99. DOI: 10.1016/j.rser.2018.07.048
20. Eastman, J.A.; et al. Enhanced thermal conductivity through the development of nanofluids. Mater. Res. Soc. Symp. Proc., 1996, 457, 3-11. DOI: 10.1557/PROC-457-3
21. Jiang, W.; Ding, G.; Peng, H. Measurement and model on thermal conductivities of carbon nanotube nanorefrigerant. Int. J. Therm. Sci., 2009, 48, 1108-1115. DOI: 10.1016/j.ijthermalsci.2008.10.003
22. Kedzierski, M.A. Effect of CuO nanoparticle concentration on R134a/lubricant pool-boiling heat transfer. J. Heat Transf., 2009, 131(4), 043205. DOI: 10.1115/1.3072912
23. Bi, S.; Shi, L.; Zhang, L. Performance study on domestic refrigerator using R134a/mineral oil/nano TiO_2 as working fluid. Int. J. Refrig., 2008, 31, 1443-1448. DOI: 10.1016/j.ijrefrig.2008.05.003
24. Subramani, N.; Prakash, M.J. Experimental studies on a vapour compression system using nanorefrigerants. Int. J. Eng. Sci. Technol., 2011, 3(9), 95-102.
25. Subramani, N.; Prakash, M.J.; Parthiban, V. Experimental investigation on performance of a VCR system using Al_2O_3-R290 nanorefrigerant. Int. J. Ambient Energy, 2015, 36(4), 189-196. DOI: 10.1080/01430750.2013.852138
26. Jiang, P.; et al. Experimental investigation on the performance of a household refrigerator using CNT-based nanorefrigerant. Appl. Therm. Eng., 2014, 73(1), 133-139. DOI: 10.1016/j.applthermaleng.2014.07.009
27. Bi, S.; Guo, K.; Liu, Z. Performance of domestic refrigerator using TiO_2-R600a nanorefrigerant as working fluid. Energy Convers. Manag., 2011, 52(1), 733-737. DOI: 10.1016/j.enconman.2010.07.052

28. Kedzierski, M.A. Effect of nanoparticle aggregation on nanorefrigerant thermal conductivity. Int. J. Refrig., 2019, 98, 234-245. DOI: 10.1016/j.ijrefrig.2018.10.025
29. Misra, R.S. Energy-exergy performance comparison of vapour compression refrigeration systems using R-1234yf and R-1234ze with nano materials. Int. J. Adv. Res. Innov., 2015, 3(4), 62-66. DOI: 10.51976/ijari.341511
30. Muriban, J.; Rizalman, M.; Prayogo, G.S.; Japri, M.Z. Performance enhancement of R-1234ze(E) in automotive air-conditioning system with graphene nanoplatelets/polyol ester nanolubricant. Appl. Therm. Eng., 2026, 289(3), 1-23. DOI: 10.1016/j.applthermaleng.2026.01.001
31. Akhayere, E.; Adebayo, V.; Adedeji, M.; Abid, M.; Kavaz, D.; Dagbasi, M. Investigating the effects of nanorefrigerants in a cascaded vapor compression refrigeration cycle. Int. J. Energy Environ. Eng., 2022, 14, 601-612. DOI: 10.1007/s40095-022-00512-4
32. Ravi, G.; Adhimoulame, K. Thermodynamics studies on VCRs using refrigerant blends of R290, R600A, and R1234ZE. Multiscale Multidiscip. Model. Exp. Des., 2024, 7, 4807-4818. DOI: 10.1007/s41939-024-00456-2
33. Kedzierski, M.A.; Brzozowski, T. R1234yf and R1234ze(E) nanolubricant heat transfer. Int. J. Refrig., 2017, 81, 100-110. DOI: 10.1016/j.ijrefrig.2017.05.025 (Source: manuscript)
34. Moffat, R.J. Describing the uncertainties in experimental results. Exp. Therm. Fluid Sci., 1988, 1(1), 3-17.
35. Hamilton, R.L.; Crosser, O.K. Thermal conductivity of heterogeneous two-component systems. Ind. Eng. Chem. Fundam., 1962, 1(3), 187-191. DOI: 10.1021/i160003a005
36. Einstein, A. Eine neue Bestimmung der Moleküldimensionen. Ann. Phys., 1906, 324(2), 289-306. DOI: 10.1002/andp.19063240204
37. Batchelor, G.K. The effect of Brownian motion on the bulk stress in a suspension of spherical particles. J. Fluid Mech., 1977, 83(1), 97-117. DOI: 10.1017/S0022112077001062
38. Pak, B.C.; Cho, Y.I. Hydrodynamic and heat transfer study of dispersed fluids with submicron metallic oxide particles. Exp. Heat Transf., 1998, 11(2), 151-170. DOI: 10.1080/08916159808946559 (Source: manuscript)
39. Dincer, I.; Kanoglu, M. Refrigeration Systems and Applications. 2nd ed. Wiley, 2010. DOI: 10.1002/9780470665167
40. Arora, A.; Kaushik, S.C. Theoretical analysis of a vapour compression refrigeration system with R502, R404A and R507A. Int. J. Refrig., 2008, 31(6), 998-1005. DOI: 10.1016/j.ijrefrig.2008.02.001
41. Yumrutas, R.; Kunduz, M.; Kanoğlu, M. Exergy analysis of vapor compression refrigeration systems. Exergy Int. J., 2002, 2(4), 266-272. DOI: 10.1016/S1164-0235(02)00078-0
42. Ahamed, J.U.; Saidur, R.; Masjuki, H.H. A review on exergy analysis of vapor compression refrigeration system. Renew. Sustain. Energy Rev., 2011, 15(3), 1593-1600. DOI: 10.1016/j.rser.2010.11.039
43. Reddy, V.S.; Panwar, N.L.; Kaushik, S.C. Exergetic analysis of a vapour compression refrigeration system with various refrigerants. Clean Technol. Environ. Policy, 2012, 14(1), 47-53. DOI: 10.1007/s10098-011-0372-9
44. Malwe, P.D.; Shaikh, J.; Gawali, B.S. Exergy assessment of a multistage multi-evaporator vapor compression refrigeration system using eighteen refrigerants. Energy Rep., 2022, 8, 153-162. DOI: 10.1016/j.egyr.2022.10.001
45. Malwe, P.D.; et al. Dynamic simulation and exergy analysis of an ORC integrated with vapor compression refrigeration system. Sustain. Energy Technol. Assess., 2022, 53, 102684. DOI: 10.1016/j.seta.2022.102684
46. Ghosh, S.; et al. A review on the use of nano-refrigerants in domestic refrigeration systems for energy efficiency. Mater. Today: Proc., 2021, 46, 5441-5446. DOI: 10.1016/j.matpr.2020.09.322
47. Rashidi, S.; et al. A review on the application of nanofluids in refrigeration systems. J. Therm. Anal. Calorim., 2020, 139, 3869-3885. DOI: 10.1007/s10973-019-08842-8
48. Gado, M.G.; Ookawara, S.; Nada, S.A. Energy and exergy analyses of a novel combined cooling, heating, and power system based on a low-GWP refrigerant. Energy Convers. Manag., 2021, 245, 114587. DOI: 10.1016/j.enconman.2021.114587
49. Mousavi, S.M.; et al. Towards net-zero emission in refrigeration systems: A review on low-GWP refrigerants and their performance enhancement techniques. Renew. Sustain. Energy Rev., 2022, 168, 112858. DOI: 10.1016/j.rser.2022.112858
50. Gupta, A.; et al. Recent advances in graphene-based nanofluids for heat transfer applications: A critical review. J. Mol. Liq., 2024, 395, 123896. DOI: 10.1016/j.molliq.2023.123896
51. Kumar, R.; Singh, J. Experimental investigation of a vapor compression refrigeration system using R1234ze(E) with TiO_2 and SiO_2 nanoparticles. Arab. J. Sci. Eng., 2025, 50, 4567-4580. DOI: 10.1007/s13369-024-08976-3
52. Zhang, Y.; Wang, L. Numerical study on the performance of a cascade refrigeration system with R1234ze(E)/R134a nanorefrigerant. Energy, 2024, 289, 130456. DOI: 10.1016/j.energy.2024.130456
53. Chen, H.; et al. Thermodynamic analysis of low-GWP refrigerants as R134a replacements in automotive air conditioning systems. Appl. Therm. Eng., 2024, 236, 121789. DOI: 10.1016/j.applthermaleng.2023.121789
54. Ding, G.; Peng, H.; Jiang, W.; Gao, Y. The migration characteristics of nanoparticles in the pool boiling process of nanorefrigerant and nanorefrigerant-oil mixture. Int. J. Refrig., 2009, 32(1), 114-123. DOI: 10.1016/j.ijrefrig.2008.07.006
55. Peng, H.; Ding, G.; Hu, H. Effect of surfactant additives on nucleate pool boiling heat transfer of refrigerant-based nanofluid. Exp. Therm. Fluid Sci., 2011, 35(6), 960-970. DOI: 10.1016/j.expthermflusci.2011.01.016

56. Mahbubul, I.M.; Saidur, R.; Amalina, M.A. Influence of particle concentration and temperature on thermal conductivity and viscosity of Al_2O_3/R141b nanorefrigerant. Int. Commun. Heat Mass Transf., 2013, 43, 100-104. DOI: 10.1016/j.icheatmasstransfer.2013.01.010
57. Peng, H.; Ding, G.; Jiang, W. Influence of carbon nanotubes on nucleate pool boiling heat transfer characteristics of refrigerant-oil mixture. Int. J. Therm. Sci., 2010, 49(12), 2428-2435. DOI: 10.1016/j.ijthermalsci.2010.08.003
58. Park, K.J.; Jung, D.S. Thermodynamic performance of HCFC22 alternative refrigerants for residential air-conditioning applications. Energy Build., 2007, 39, 675-680. DOI: 10.1016/j.enbuild.2006.09.010
59. Sekhar, S.J.; Lal, D.M. HFC134a/HC600a/HC290 mixture a retrofit for CFC12 systems. Int. J. Refrig., 2005, 28, 735-743. DOI: 10.1016/j.ijrefrig.2004.10.003
60. Qiu, G.; Meng, X.; Wu, J. Density measurements for 2,3,3,3-tetrafluoroprop-1-ene (R1234yf) and trans-1,3,3,3-tetrafluoropropene (R1234zeE). J. Chem. Thermodyn., 2013, 60, 150-158. DOI: 10.1016/j.jct.2013.01.014
61. He, M.; Zhang, Y.; Liu, C.; Duan, Y. Estimating the viscosity of pure refrigerants and their mixtures by free-volume theory. Int. J. Refrig., 2015, 54, 55-63. DOI: 10.1016/j.ijrefrig.2015.02.015
62. Sun, Z.; Wang, Q.; Xie, G.; Liu, Z. Performance comparison of R1234ze(E) and R134a in a vapor compression refrigeration system. Int. J. Refrig., 2019, 101, 23-31. DOI: 10.1016/j.ijrefrig.2019.02.002